International Journal of Applied Engineering Research ISSN 0973-4562 Volume 12, Number 23 (2017) pp. 13201-13206

Structural, electrical and magnetic properties of Mg doped Ni-Cu-Zn nanoferrites synthesized by Citrate Precursor method

Biju Thangjam

Research Scholar, Department of Physics, National Institute of Technology Manipur, Lamphelpat, Langol Road, Imphal, Manipur 795004, India and Assistant Professor, Department of Physics, Dhanamanjuri College of Science, Imphal, Manipur 795001, India. (Affiliated to Manipur University, Canchipur, Imphal, Manipur 795003, India.)

Orcid Id: 0000-0002-4661-4513

Ibetombi Soibam

Assistant Professor, Department of Physics, National Institute of Technology Manipur, Lamphelpat, Langol Road, Imphal, Manipur 795004, India.

Orcid Id: 0000-0001-9644-7349

Abstract

A series of NiMgCuZn nanoferrites having chemical formula $Ni_{0.5-x}Mg_xCu_{0.3}Zn_{0.2}Fe_2O_4$ (where x=0.05,0.10,0.15,0.20) were successfully synthesized by the citrate precursor method. These nanoferrites were sintered by conventional technique. X-ray diffraction analysis confirmed the formation of single cubic spinel phase in these nanoparticles. Crystallite size was estimated and was found to lie in the range of 44nm-52nm. Structural properties like lattice constant, grain size and density have been studied. Room temperature dielectric studies revealed low dielectric constant and low dielectric loss values. Resistivity values were enhanced with Mg doping up to a particular concentration. Evaluation of room temperature magnetic behaviour of these Mg substituted NiCuZn nanoferrites showed moderate initial permeability values. FT-IR spectra showed two strong absorption bands in the range of wave numbers 400-600cm^{-1}, which are characteristic of spinel ferrites. The sinterability at low temperature and the attainability of low values of dielectric loss and high resistivity ($10^7\Omega$-cm) may render these nanoferrites suitable for multilayer chip inductor (MLCI) applications.

Keywords: NiMgCuZn nanoferrites, citrate precursor method, dielectric properties, FT-IR, initial permeability.

INTRODUCTION

The tremendous advancement in the fields of information technology and mobile communication has resulted in a great demand for miniaturization of many latest electronic products including cellular phones, notebook computers, video cameras, etc. [1,2]. In recent years, surface mounting devices like multilayer chip inductors (MLCI) have been designed to satisfy such requirements. Nanocrystalline spinel ferrites like Ni-Cu-Zn nanoferrites have been the most universal ferrite materials for MLCI due to their low sintering temperature, high electrical resistivity, high permeability, hard mechanical properties and also high Curie temperature [3,4]. Doping with Mg may improve the electromagnetic properties of Ni-Cu-Zn ferrite samples. This is because of the fact that Mg containing composition may avoid the tendency of discontinuous grain growth [1].

The synthesis of fine reactive ferrite powder is essential for MLCI technology. Various wet-chemical methods can be adopted for the preparation of ultrafine powder. The citrate precursor method is one such method which has the advantages of obtaining nanocrystalline ferrite particles, homogeneous distribution of ions at the atomic level, good control of stoichiometry, low temperature synthesis, high efficiency, etc. [5]. Hence, citrate precursor method has been adopted for the synthesis of the nanoferrite samples under investigation.

METHODS

Nanocrystalline ferrite powders having chemical formula $Ni_{0.5-x}Mg_xCu_{0.3}Zn_{0.2}Fe_2O_4$ (where x=0.05,0.10,0.15,0.20) were prepared by the citrate precursor method using nickel nitrate ($Ni(NO_3)_2.6H_2O$) (Merck, India), magnesium nitrate ($Mg(NO_3)_2.6H_2O$) (Merck, India), copper nitrate ($Cu(NO_3)_2.3H_2O$) (Merck, India), zinc nitrate ($Zn(NO_3)_2.6H_2O$) (Merck, India), ferric nitrate ($Fe(NO_3)_3.9H_2O$) (Merck, India) and citric acid ($C_6H_8O_7$) (Merck, India). The stoichiometric amounts of metal nitrates and citric acid were dissolved in double distilled water. Metal nitrate solutions were mixed with citric acid solution in 1:1 molar ratio of nitrate to citric acid. The pH of the solution was maintained at 7 using ammonia solution. Then the solution was heated at 100°C to transform into a thick gel. Thereafter, the gel ignited and burnt with glowing flints yielding loose ferrite powder. The as-burnt powder was granulated using 10% polyvinyl alcohol as a binder and was pressed to form pellets (10mm diameter) and toroidal rings (30mm outer diameter, 10mm inner diameter and 3mm thickness) by applying a pressure of 10 ton cm^{-2}. These specimens were pre-sintered at 600°C for 4h in a programmable conventional furnace to expel the binder and were then subjected to final sintering at 900°C for 2h using the above mentioned furnace at

a heating rate of 5°C/min. The samples were furnace cooled. One set of pellets was coated with silver paste to provide electrical contact for electrical measurements and the toroidal rings were wound with 70 turns of 30 SWG enamelled copper wire to form toroids.

For the phase and crystal structure identification of the samples, the X-ray diffraction patterns were recorded using X-Pert Pro PANalytical X-ray diffractometer with CuKα radiation (λ=1.5406Å). Dielectric constant and initial permeability values were calculated from the capacitance and inductance measured respectively in the frequency range of 20Hz to 2MHz at room temperature by employing a precision LCR meter E4980A. The micrographs of the samples were examined by scanning electron microscope (SEM) model Jeol JSM 6360. FT-IR spectra were recorded using Perkin Elmer Spectrum1 FT-IR Spectrometer in the wavenumbers ranging from 450-4000 cm^{-1}.

RESULTS AND DISCUSSION

XRD Analysis

X-ray diffraction patterns of the ferrite samples $Ni_{0.5-x}Mg_xCu_{0.3}Zn_{0.2}Fe_2O_4$ are shown in Figure1. The most intense peaks in all the specimens indexed as (220), (311), (222), (400), (422), (333) and (440) are found to match well with single-phase cubic spinel (JCPDS card no. 01-071-3850). No other peaks corresponding to other phases or impurities are observed. The XRD parameters like lattice constant, X-ray density and crystallite size for all the specimens are tabulated in Table 1. The increase in lattice constant with increase in Mg^{2+} content is due to the higher ionic radii of Mg^{2+} ions (0.72Å) as compared to that of Ni^{2+} ions (0.69Å) [6]. This lattice expansion is revealed in the XRD patterns by a slight shift in the peak positions towards lower diffraction angles [7]. The crystallite size of the ferrites was calculated from the most intense peak (311) by using Debye-Scherrer's relation:

$$t = 0.9\lambda / \beta\cos\theta \quad (1)$$

where, λ = X-ray wavelength, β = full width at half maximum, θ = Bragg's diffraction angle. The decreasing trend of crystallite size due to Mg^{2+} incorporation could be explained on the basis of crystal growth process in a solution, which depends on many factors. The two most important ones are: (i) the molecular concentration of the material approaching the surface of the tiny crystal during the growth process and (ii) the site preferences of the cations in the ferrite system. In the case of the first factor, the local temperature is usually higher than the solution temperature on account of the liberation of latent heat at the surface. The surface temperature affects the molecular concentration at the surface of the crystal and, hence, the crystal growth rate. In the second case, the grain growth is obstructed when the cation preferences are not fully satisfied. Thus, we can say that as the Mg content increases, more heat may be liberated. This leads to a decrease in molecular concentration at the crystal surface and hence obstructs the grain growth [6].

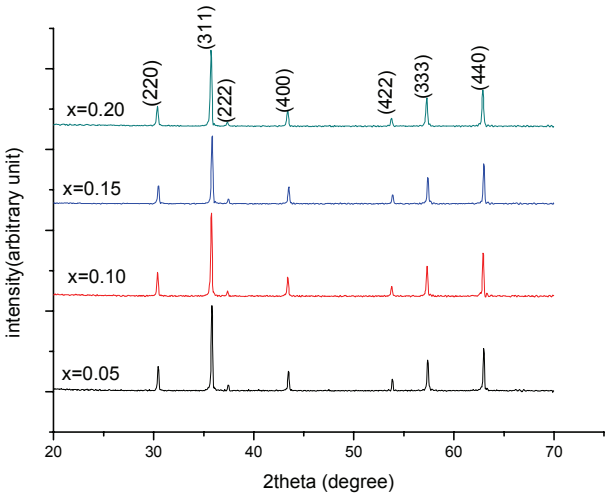

Figure 1: XRD patterns of $Ni_{0.5-x}Mg_xCu_{0.3}Zn_{0.2}Fe_2O_4$ ferrites.

X-ray densities (d_x) for different compositions were calculated using the formula:

$$d_x = 8M/NV \quad (2)$$

where, N = Avogadro's number, M = molecular weight of the sample, V = volume of the unit cell. The X-ray density is expected to decrease with Mg^{2+} incorporation because the lattice parameter increases with Mg^{2+} content. The decrease in X-ray density can be accounted by the fact that the density and atomic weight of Mg^{2+} (1.74 and 24.31 gm/cm^3) are lower than those of Ni^{2+} (8.90 and 58.69 gm/cm^3) and Fe^{3+} (7.86 and 55.85 gm/cm^3) [8]. The bulk densities of the samples were calculated from the relation:

$$d_b = m/\pi r^2 l \quad (3)$$

where, m = mass, r = radius and l = thickness of the pellet.

Microstructural characterization

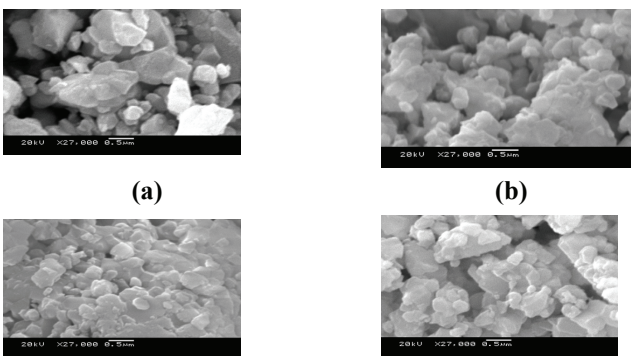

Figure 2: SEM images of (a) x=0.05, (b) x=0.10, (c) x=0.15 and (d) x=0.20 for $Ni_{0.5-x}Mg_xCu_{0.3}Zn_{0.2}Fe_2O_4$ ferrites.

Figure 2 shows scanning electron microscope (SEM) micrographs of the sintered samples $Ni_{0.5-x}Mg_xCu_{0.3}Zn_{0.2}Fe_2O_4$. The average grain size decreases with increasing Mg^{2+} content. The declining trend of average grain size could be due to the presence of MgO, which acts as a microstructural stabilizer, responsible for finer and more uniform grain size. Nevertheless, MgO is a stable oxide which prevents the tendency of discontinuous grain growth [9].

Electrical properties

The dielectric constant of the $Ni_{0.5-x}Mg_xCu_{0.3}Zn_{0.2}Fe_2O_4$ nanoparticles with varying log frequency at room temperature are shown in Figure 3. The dielectric constant (ε′) has been calculated by using the relation:

$$\varepsilon' = Ct/ \varepsilon_0 A \qquad (4)$$

where, C = capacitance, t = thickness, A = area of cross section of the pellet and ε_0 = permittivity of free space (8.85 x $10^{-12}Fm^{-1}$). Dielectric constant in ferrites is influenced by various factors such as micro-structural arrangement, cation distribution, density and charge polarization. The decrease of dielectric constant with increasing frequency is a normal dielectric behavior of spinel ferrites. The phenomenon of dielectric dispersion in ferrites is analogous to Maxwell-Wagner interfacial polarization and in agreement with Koops phenomenological theory [10,11]. This dispersion phenomenon can be explained on the basis of space charge polarization which is due to the presence of highly conducting grains separated by poorly conducting grain boundaries of a dielectric causing localized accumulation of charges under the influence of an electric field. Hence, at lower frequencies, the grain boundaries are more effective than grains in electrical conduction. Thinner the grain boundary, the higher is the value of dielectric constant[12]. The polarization mechanism in ferrites is similar to the conduction process. The polarization at lower frequencies may result from the electron hopping between Fe^{3+} and Fe^{2+} ions in the ferrite lattice. The polarization decreases with increasing frequency and reaches

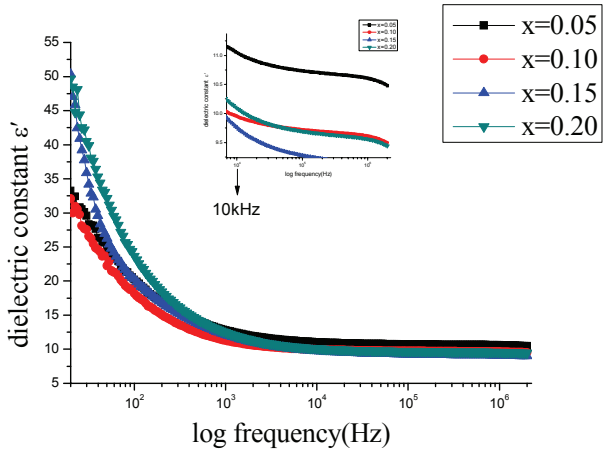

Figure 3: Frequency dependence of dielectric constant (ε′) for $Ni_{0.5-x}Mg_xCu_{0.3}Zn_{0.2}Fe_2O_4$ ferrites.

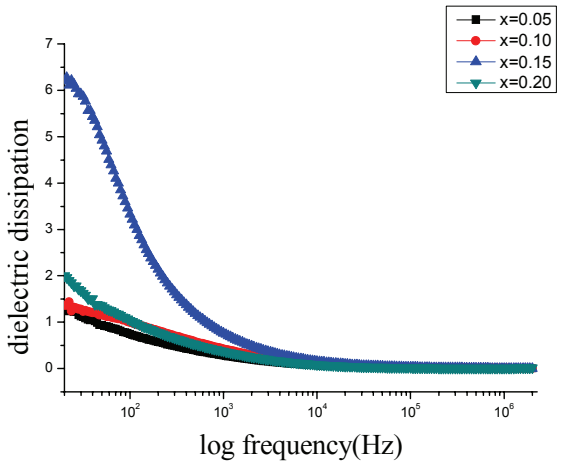

Figure 4: Variation of dielectric dissipation with log frequency for $Ni_{0.5-x}Mg_xCu_{0.3}Zn_{0.2}Fe_2O_4$ ferrites.

a constant value because of the reason that beyond a certain frequency of external field, the electron exchange between Fe^{3+} and Fe^{2+} ions cannot follow the alternating field [13, 14]. Density also plays an important role in the process of polarization. This can be explained by the fact that increase in density decreases the porosity resulting in greater number of polarizing species per unit volume [5]. Accordingly, it is observed that dielectric constant decreases with decrease in density as given in Table 1. Further, Mg^{2+} ions have strong preference for B-sites although a few have preference to occupy the A-sites [9]. The tendency of Mg^{2+} ions to occupy the B-sites will result in the migration of Fe^{3+} ions to the A-sites leading to slowing down of the electron transfer between Fe^{3+} and Fe^{2+} ions in the B-sites, thereby decreasing the polarization. Accordingly, dielectric constant decreases with Mg^{2+} content. However, the increase in dielectric constant for the Mg^{2+} content of 0.20 might be due to the occupancy of tetrahedral sites by the Mg^{2+} ions for this composition, which might lead to the migration of Fe^{3+} ions to the octahedral sites, thereby enhancing the electron hopping process between the Fe^{3+} and Fe^{2+} ions in the B-sites.

Figure 4 shows the variation of dissipation factor as a function of logarithmic frequency in the range from 20Hz to 2MHz at room temperature for $Ni_{0.5-x}Mg_xCu_{0.3}Zn_{0.2}Fe_2O_4$ (x =0.05, 0.10, 0.15 and 0.20) nanoparticles. The high value of dielectric loss at lower frequencies corresponds to high value of resistivity due to grain boundaries. Hence, more energy is required for electron exchange between Fe^{2+} and Fe^{3+} ions at the octahedral sites resulting in high value of energy loss. The high frequency region corresponds to a low value of resistivity due to the grains. Therefore, a small amount of energy is required for the electron transfer between Fe^{2+} and Fe^{3+} ions resulting in small energy loss [15]. Dielectric properties such as dielectric constant and dielectric loss are important for MLCI applications especially in the high frequency range. These ferrites possess relatively low dielectric loss and low dielectric constant values rendering them suitable for core materials in MLCIs with high performance [4].

Table 1: Lattice constant, X-ray density, experimental density, crystallite size, resistivity and dielectric constant values of $Ni_{0.5-x}Mg_xCu_{0.3}Zn_{0.2}Fe_2O_4$ ferrites.

Sample 'x'	0.05	0.10	0.15	0.20
Lattice constant (Å)	8.304	8.308	8.320	8.326
X-ray density (gm/cm^3)	5.45	5.42	5.35	5.29
Experimental density (gm/cm^3)	4.45	4.09	4.06	4.32
Crystallite size (nm)	51.57	50.39	45.98	44.35
Resistivity (Ω-cm)	$1.84x10^7$	$4.89x10^7$	$6.85x10^7$	$1.75x10^7$
Dielectric constant at 10kHz	11.05	9.95	9.76	10.09

Electrical resistivity is an important property of low temperature sintered ferrites for MLCI application. Variation of dc resistivity of $Ni_{0.5-x}Mg_xCu_{0.3}Zn_{0.2}Fe_2O_4$ ferrite with composition is shown in Table 1. These values are appreciably high, rendering them suitable for high frequency applications. It is reported that there is an inverse proportionality between resistivity and dielectric constant [16]. A relatively low resistivity has also been found to be associated in $Ni_{0.4}Zn_{0.6}Fe_2O_4$ ferrites with a high dielectric constant [17].

FT-IR Measurements

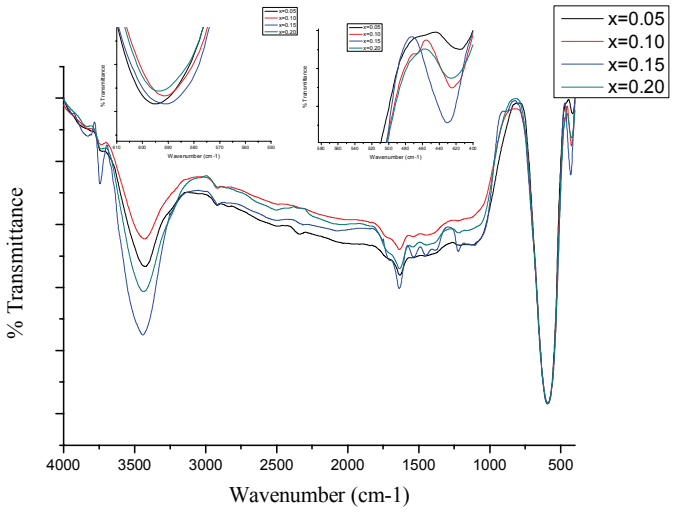

Figure 5: FT-IR spectra of $Ni_{0.5-x}Mg_xCu_{0.3}Zn_{0.2}Fe_2O_4$ ferrites.

The FT-IR spectroscopy is an effective technique in establishing the cation distribution in a crystal lattice through their vibrational modes [18]. The FT-IR spectra of the ferrite samples $Ni_{0.5-x}Mg_xCu_{0.3}Zn_{0.2}Fe_2O_4$ are shown in Figure 5. Two strong bands (ν_1 and ν_2) within the range of 590-594 cm^{-1} and 415-430cm^{-1} are characteristic of the spinel structure and corresponds to the vibrations of the metal ion-oxygen complexes in the tetrahedral and octahedral sites respectively [19, 20].

The FT-IR spectra exhibit prominent bands in the range of wave numbers 3423–3442 cm^{-1} and 1633–1637 cm^{-1} which are attributed to the tensional stretching modes and H-O-H bending vibration of the free or absorbed water molecules [21].

It is observed that the frequency band ν_2 shifts towards higher wavenumber side with increasing Mg^{2+} content up to x = 0.15. This can be accounted by the fact that Mg^{2+} ions might be occupying the octahedral sites. As Mg^{2+} ions have larger ionic radius than Fe^{3+} ions (0.55Å), they push the Fe^{3+} ions towards oxygen ion resulting in decreased Fe^{3+}- O^{2-} bond length. This is so because there is an inverse relationship between wavenumber and bond length [9].

Magnetic properties

Initial magnetic permeability

The variation in real part of the initial permeability, μ_i' with log frequency for different ferrite compositions $Ni_{0.5-x}Mg_xCu_{0.3}Zn_{0.2}Fe_2O_4$ are shown in Figure 6. Real part of permeability depends on many factors like stoichiometry, grain structure, composition, impurity contents, crystal anisotropy, saturation magnetization, porosity, etc. Large grain size, high saturation magnetization, low crystal anisotropy, low porosity and high purity of the material are favourable conditions for higher values of permeability [22, 23]. Permeability of polycrystalline ferrites is related to two mechanisms: domain wall motion and spin rotation:

$$\mu_i = 1 + \chi_w + \chi_{spin} \quad (5)$$

where, χ_w is the domain wall susceptibility and χ_{spin} is intrinsic rotational susceptibility. They may be written as

$$\chi_w = 3\pi M_s^2 D/4\gamma \quad (6)$$

$$\chi_{spin} = 2\pi M_s^2/K \quad (7)$$

where, M_s is the saturation magnetization, K the anisotropy constant, D the average grain diameter, and γ the domain wall energy [24]. Out of these two mechanisms, the energy required for domain wall displacement being lower than that required for domain rotation, magnetization due to the former process is greater [25]. As can be seen from relations (5) and (6), initial permeability is greatly affected by the grain size and saturation magnetization. In the present investigation also, it is observed that μ_i' varies linearly with grain size as shown in Table 2 . Grain boundary diminishes with increasing grain size leading to easy movement of domain walls, which ultimately enhances the initial permeability [26]. Hence, initial permeability is found to decrease with decreasing grain

size. Dimri etal [25] also reported that formation of domain walls is not energetically favoured in small grains leading to lower initial permeability in small grains. Further, they also reported that increase in density leads to decrease in intragranular porosity, which reduces the demagnetizing field due to the pores, thereby resulting in continuous flux propagation, which consequently increases the permeability. This reasoning supports the present study in which initial permeability decreases with reduction in bulk density for Mg^{2+} content up to 0.15. Increase in experimental density for Mg^{2+} concentration of 0.2 will account for the rise in the value of initial permeability for this concentration.

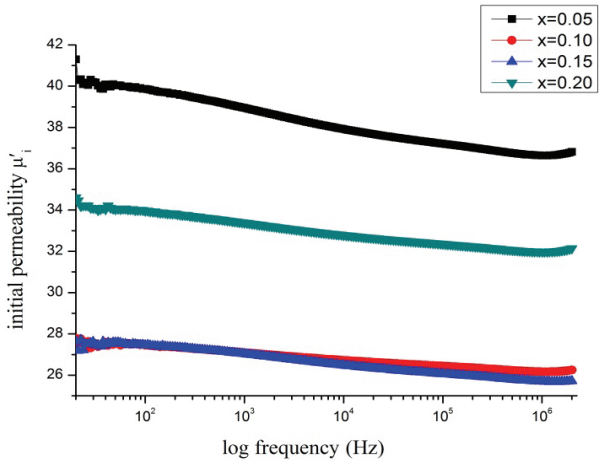

Figure 6: Initial permeability versus log frequency for $Ni_{0.5-x}Mg_xCu_{0.3}Zn_{0.2}Fe_2O_4$ ferrites.

A slight drop in the values of permeability with increasing frequency is observed at higher frequencies for all the compositions. This can be accounted by the fact that at high frequencies, the unpinning of the domain walls cannot keep pace with the rapidly changing magnetic field resulting in diminishing value of μ_i' [27]. The resonance peaks usually observed [26] could not be seen in the present investigation, which might be due to the fact that they probably occur beyond the measured frequency range. The observed permeability values are higher and more stable than those reported elsewhere [5]. Stability of μ_i' over a large frequency range is a desirable characteristic feature for various applications such as broadband pulse transformers [28] and wide band read-write heads for video recording devices [22, 29].

Table 2: Grain size, initial permeability, tetrahedral band and octahedral band of $Ni_{0.5-x}Mg_xCu_{0.3}Zn_{0.2}Fe_2O_4$ ferrites.

Samples	Grain size	Initial permeability	Tetrahedral	Octahedral
'x'		at 10kHz	band, ν_1	band, ν_2
	(μm)		(cm^{-1})	(cm^{-1})
0.05	1.098	37.92	594	415
0.10	0.526	26.72	591	424
0.15	0.468	26.48	590	430
0.20	0.575	32.78	593	425

CONCLUSIONS

Nanocrystalline $Ni_{0.5-x}Mg_xCu_{0.3}Zn_{0.2}Fe_2O_4$ samples with crystallite size ranging from 44 nm to 52 nm and low dielectric constant values below 12 at 10kHz were synthesized by citrate precursor method. XRD analysis of these ferrites exhibited that all the samples have single phase spinel structure. It was observed that lattice constant increases while XRD density decreases with increasing Mg^{2+} concentration. The dielectric constant and initial permeability values were found to decrease with Mg^{2+} incorporation upto a concentration of x=0.15. Sinterability at low temperature, attainability of high resistivity and low dielectric loss values, along with the stability of μ_i' over a large frequency range may render these magnetic nanoparticles applicable for broadband pulse transformers, wide band read-write heads for video recording devices and multilayer chip inductors.

ACKNOWLEDGEMENT

The authors are thankful to MANIPUR UNIVERSITY for the XRD measurements, NEHU for the SEM measurements and IIT Madras for the FT-IR measurements.

REFERENCES

[1] M.A. Gabal. "Effect of Mg substitution on the magnetic properties of NiCuZn ferrite nanoparticles prepared through a novel method using egg white", *Journal of Magnetism and Magnetic Materials*, vol.321, pp. 3144 – 3148, 2009.

[2] T. Krishnaveni, B.R. Kanth, V.S.R. Raju, and S.R. Murthy. "Fabrication of multilayer chip inductors using Ni-Cu-Zn ferrites", *Journal of Alloys and Compounds*, vol. 414, pp. 282 – 286, 2006.

[3] H. Harzali, F. Saida, A. Marzouki, A. Megriche, F. Baillon, F. Espitalier and A. Mgaidi, "Structural and magnetic properties of nano-sized NiCuZn ferrites synthesized by co-precipitation method with ultrasound irradiation", *Journal of Magnetism and Magnetic Materials* , vol. 419, pp. 50 – 56, 2016.

[4] M.P. Reddy, G. Balakrishnaiah, W. Madhuri, M.V. Ramana, N.R. Reddy, K.V. Siva Kumar, V.R.K. Murthy and R.R. Reddy. "Structural, magnetic and electrical properties of NiCuZn ferrites prepared by microwave sintering method suitable for MLCI applications", *Journal of Physics and Chemistry of Solids*, vol. 71, pp. 1373 – 1380, 2010.

[5] B. Thangjam and I. Soibam. "Comparative Study of Structural, Electrical and Magnetic Behaviour of Ni-Cu-Zn Nanoferrites sintered by Microwave and Conventional Techniques", *Journal of Nanomaterials*, vol. 2017, Article ID 5756197, 10 pages, 2017.

[6] M.M. Eltabey, A.M. Massoud and C. Radu. "Microstructure and Superparamagnetic Properties of Mg-Ni-Cd Ferrites Nanoparticles", *Journal of*

Nanomaterials, vol. 2014, Article ID 492832, 7 pages, 2014.

[7] P. Yadoji, R. Peelamedu, D. Agrawal and R. Roy. "Microwave sintering of Ni-Zn ferrites: comparison with conventional sintering", *Materials Science and Engineering B*, vol. 98, pp. 269 – 278, 2003.

[8] T. Vigneswari and P. Raji. "Structural and magnetic studies of magnesium substituted nickel ferrite nanoparticles by citrate precursor method", *Journal of Ceramic Processing Research*, vol. 17(9), pp. 999 – 1005, 2016.

[9] Ch. Sujatha, K.V. Reddy, K.S. Babu, A.R.C. Reddy and K.H. Rao. "Structural and magnetic properties of Mg substituted NiCuZn Nano ferrites", *Physica B*, vol. 407, pp. 1232 – 1237, 2012.

[10] Md.D. Rahaman, K.K. Nahar, M.N.I. Khan and A.K.M.A. Hossain. "Synthesis, structural and electromagnetic properties of $Mn_{0.5}Zn_{0.5-x}Mg_xFe_2O_4$ (x=0.0, 0.1) polycrystalline ferrites", *Physica B*, vol. 481, pp. 156 – 164, 2016.

[11] J. Balavijayalakshmi, N. Suriyanarayanan and R. Jayaprakash. "Role of copper on structural, magnetic and dielectric properties of nickel ferrite nano particles", *Journal of Magnetism and Magnetic Materials* vol. 385, pp. 302 – 307, 2015.

[12] P.S. Das and G.P. Singh. "Structural, magnetic and dielectric study of Cu substituted NiZn ferrite nanorod", *Journal of Magnetism and Magnetic Materials* , vol.401, pp. 918 – 924, 2016.

[13] A.A. Kadam, S.S. Shinde, S.P. Yadav, P.S. Patil and K.Y. Rajpure. "Structural, morphological, electrical and magnetic properties of Dy doped Ni-Co substitutional spinel ferrite", *Journal of Magnetism and Magnetic Materials* , vol. 329, pp. 59 – 64, 2013.

[14] I. Soibam. "A Study of Microwave sintered Ni substituted Lithium Zinc Ferrite synthesized by Citrate Precursor method", *International Journal of Materials Science and Engineering*, vol. 4(1), pp. 54 – 59, 2016.

[15] K.M. Batoo and Md.S. Ansari. "Low temperature - fired Ni-Cu-Zn ferrite nanoparticles through auto-combustion method for multilayer chip inductor applications", *Nanoscale Research Letters*, 7:112, 2012.

[16] A. Thakur and M. Singh. "Preparation and characterization of nanosize $Mn_{0.4}Zn_{0.6}Fe_2O_4$ ferrite by citrate precursor method", *Ceramics International*, vol. 29, pp. 505 – 511, 2003.

[17] J. Smit and H.P.J. Wijn. "Ferrites". Cleaver-Hume Press Ltd., London, Chap. XII, 1959.

[18] Z.K. Heiba, Md. B. Mohamed, L. Arda and N. Dogan. "Cation distribution correlated with magnetic properties of nanocrystalline gadolinium substituted nickel ferrite", *Journal of Magnetism and Magnetic Materials* , vol. 391, pp. 195-202, 2015.

[19] M. Khairy and M.E. Gouda. "Electrical and optical properties of nickel ferrite / polyanilina nanocomposite", *Journal of Advanced Research*, vol. 6, pp. 555 – 562, 2015.

[20] B. Thangjam and I. Soibam. "FT-IR study of Cu substituted Ni-Zn ferrites prepared by citrate precursor method", *Advanced Materials Proceedings*, vol. 2(3), pp. 205 – 208, 2017.

[21] J. Xiang, X. Shen, F. Song and M. Liu. "One-Dimensional NiCuZn ferrite nanostructures: Fabrication, structure and magnetic properties", *Journal of Solid State Chemistry*, vol. 183, pp. 1239 – 1244, 2010.

[22] V. J. Angadi, B. Rudraswamy, K. Sadhana and K. Praveena. "Structural and magnetic properties of manganese zinc ferrite nanoparticles prepared by solution combustion method using mixture of fuels", *Journal of Magnetism and Magnetic Materials*, vol. 409, pp. 111 – 115, 2016.

[23] J. Smit and H.P.J. Wijn. "Ferrites", Cleaver Hume Press Ltd., London, Chap. XIII, 1959.

[24] A.K.M. Akther Hossain, K.K. Kabir, M. Seki, T. Kawai and H. Tabata. "Structural, AC, and DC magnetic properties of $Zn_{1-x}Co_xFe_2O_4$", *Journal of Physics and Chemistry of Solids*, vol. 68, pp. 1933 – 1939, 2007.

[25] M.C. Dimri, A. Verma, S.C. Kashyap, D.C. Dube, O.P. Thakur and C. Prakash. "Structural, dielectric and magnetic properties of NiCuZn ferrite grown by citrate precursor method", *Materials Science and Engineering B*, vol. 133, pp. 42 – 48, 2006.

[26] T. Jahanbin, M. Hashim and K.A. Mantori. "Comparative studies on the structure and electromagnetic properties of Ni-Zn ferrites prepared via co-precipitation and conventional ceramic processing routes", *Journal of Magnetism and Magnetic Materials*, vol. 322, pp. 2684 – 2689, 2010.

[27] A. Verma, T.C. Goel and R.G. Mendiratta. "Frequency variation of initial permeability of NiZn ferrites prepared by the citrate precursor method", *Journal of Magnetism and Magnetic Materials*, vol. 210, pp. 274 – 278, 2000.

[28] B.D. Cullity and C.D. Graham. "Introduction To Magnetic Materials", John Wiley & Sons, Hoboken, Chap. 13, 2009.

[29] A. Verma and R. Chatterjee. "Effect of zinc concentration on the Structural, electrical and magnetic properties of mixed Mn-Zn and Ni-Zn ferrites synthesized by the citrate precursor technique", *Journal of Magnetism and Magnetic Materials*, vol. 306, pp. 313 – 320, 2006.